



# Vibrational characteristics of size-dependent vibrating ring gyroscope

A. Karimzadeh<sup>a</sup> and M.T. Ahmadian<sup>b,\*</sup>

a. *School of Mechanical Engineering, Sharif University of Technology, Tehran, Iran.*

b. *School of Mechanical Engineering; Center of Excellence in Design, Robotics and Automation, Sharif University of Technology, Tehran, Iran.*

Received 24 January 2018; accepted 14 May 2018

## KEYWORDS

Natural frequency;  
 Modified couple stress theory;  
 Vibrating ring gyroscope;  
 Pull-in voltage;  
 Static deflection.

**Abstract.** In this paper, vibrational analysis of a size-dependent micro-ring gyroscope under electrostatic DC voltage is performed. Governing equations of size-dependent micro rings and corresponding finite-element formulation of circular micro ring along with eight half circular stiffeners embedded inside the ring are derived based on the modified couple stress theory, Hamilton's principle, and in-extensionality approximation. Frequency analysis indicates that the obtained mode shape of the ring gyroscope is slightly different from the one previously reported in the literature. Size-dependent behavior of the gyroscope is studied, and related findings confirm the gap between classic and non-classic natural frequencies and pull-in voltage when the ring thickness is in order of material length scale parameter. Two different orientations for the actuation electrodes of the micro-ring gyroscope are implemented, and the effect of these orientations on the static deflection, pull-in instability, and device frequencies in the sense ( $45^\circ$  direction) and drive ( $0^\circ$  direction) directions is investigated. Results reveal that the pull-in phenomena take place under lower voltages for  $0^\circ$  and  $45^\circ$  orientation of electrodes in comparison with  $0^\circ$  orientation; frequency split occurs in higher voltages for  $0^\circ$  and  $45^\circ$  orientation. A comparison between finite-element numerical natural frequencies of single ring and previously obtained analytical ones shows excellent agreement.

© 2018 Sharif University of Technology. All rights reserved.

## 1. Introduction

Because of simplicity in construction and usage as well as high precision [1], Micro-Electro-Mechanical Systems (MEMS), such as micro switches [2,3], micro-resonators [4], energy harvesters [5,6], and gyroscopes [7], are developed for different industrial uses. Micro accelerometers and micro gyroscopes are two of

the most practical MEMS devices that measure the translational and rotational speed rates of systems, respectively [7,8]. A Coriolis gyroscope, as a micro gyroscope, works based on the generated Coriolis force, and it is classified into three major subsets: tuning fork gyroscope [9], beam gyroscope [10], and vibrating ring gyroscope [11]. Vibrating ring gyroscope is a rotating ring connected to a number of stiffeners (usually 8 or 16) and actuated by electrostatic force [7].

Different types of vibrating ring gyroscopes have been manufactured and tested by researchers [11-13]. The first generation of the vibrating ring gyroscopes was designed by Putty [14]. This gyroscope is made of a nickel-based vibrating ring, suspended on sixteen half

\*. *Corresponding author. Tel.: +98 21 66165503*  
*E-mail addresses: a-karimzadeh@fasau.ac.ir (A. Karimzadeh); ahmadian@sharif.edu (M.T. Ahmadian)*

circular stiffeners and actuated by electrostatic force in both actuation and sense modes. Low-quality factor and high thermal sensitivity are the main disadvantages of this sensor. Ayazi and Najafi [11] designed and fabricated a similar, highly functional silicon-based gyroscope, which is of lower thermal sensitivity. They considered eight half circular stiffeners, and showed that the performance of the gyroscope improved in the new design. Weng et al. [15] designed a novel accelerometer and a vibrating ring sensor capable of measuring the rotation rate and linear acceleration of the devices at the same time. They used finite element method to analyze the sensor. Designing and testing a novel piezoelectric based vibrating ring was performed by Tao et al. [12]. In this gyroscope, beams are used instead of circular stiffeners, and piezoelectric effect is utilized in drive and sense directions instead of the electrostatic force.

Elastic rings are the main components of vibrating ring gyroscopes; therefore, many researchers modeled and analyzed the mechanical behavior of these components [16-19]. Wu and Parker [16] presented the natural frequency analysis of rings resting on the general elastic foundation. They considered two sets of orthogonal stiffeners in an arbitrary direction. The vibrational analysis of extensional and in-extensional rotating rings based on the wave propagation approach was performed by Huang et al. [20]. Cooley and Parker [17] also carried out the vibrational analysis of the rotating rings. They investigated the high speed rate of rotation along with the discrete stiffeners in their model. Bisegna and Caruso [21] studied the dynamic behavior of the imperfect vibrating rings by considering perturbations of the mass density and bending stiffness of a perfect ring. They obtained the frequency split of the rings, and showed that their results were in good agreement with analytical findings.

Due to the small size of micro scale structures, the size-dependency effect plays an important role in the mechanical response of these systems; hence, the mechanical behavior of these components cannot be explained and justified by the classical continuum theory [22-24]. On the other hand, non-classic theories, such as modified couple stress theory [25], can accurately model the micro scale structures and cover the gap between the experimental and classical results. Due to the capability of the modified couple stress theory in modelling of micro scale structures, many researchers have utilized this theory to model the static and dynamic behaviors of micro electromechanical systems [26-28]. The static and dynamic behaviors of micro cantilevers on the basis of the modified couple stress theory were studied by Rahaeifard et al. [27]. They obtained the pull-in voltage of these systems, and found that the size-dependent results were in

good agreement with the experimental observations performed by Osterberg and Senturia [29]. Abbasnejad et al. [30] obtained the static and dynamic pull-in voltages of size-dependent FGM micro beams under electrostatic force and investigated the stability of these structures. Based on the modified couple stress theory, vibrational analysis and nonlinear pull-in instability of micro plates were studied by Wang et al. [31]. Their findings revealed that the effects of the material length scale parameter and surface energy became more significant as the beam thickness decreased. Kim and Reddy [26] analyzed size-dependent functionally graded plates based on the third-order shear deformation theory. They used finite-element method to investigate the effect of modified couple stress theory and geometric nonlinearities. The quasi static and dynamic governing equations of the viscoelastic micro beams using the modified couple stress theory were derived by Zhang and Fu [32]. They utilized Galerkin method to obtain the pull-in voltage of the system and validated the results with FEM model. Rahaeifard and Mojahedi [33] investigated the effect of mechanical shock on the dynamic behavior of micro accelerometers. They used finite-element and multiple time scale methods to obtain the response of the system, and showed that using the modified couple stress theory in comparison with classical continuum beam theory can change the response of the system from unstable to stable.

The present paper deals with the effect of the electrostatic DC voltage on the static deflection, pull-in instability, and natural frequencies of the size-dependent ring gyroscope (ring with eight discrete half circular stiffeners embedded inside the ring) in the absence of angular velocity. Based on the modified couple stress theory, the micro rings' governing equations of motion are derived, and the corresponding in-extensional ring element is proposed. By using the proposed ring element, the complete finite-element formulation of the vibrating ring gyroscope structure is presented. By utilizing the finite-element model, the natural frequency, static deflection, and pull-in instability of the system under electrostatic DC voltage can be studied. Two different orientations for the actuated electrodes of the micro ring gyroscope are implemented, and effect of these orientations on the static deflection, device frequencies, and pull-in instability is investigated. The size-dependent behavior of the gyroscope is investigated, and findings are compared to classical ones.

## 2. Modeling of circular rings

According to Figure 1, the displacement field of in-plane motion of micro-ring based on the Euler-Bernoulli beam theory in the cylindrical coordinate

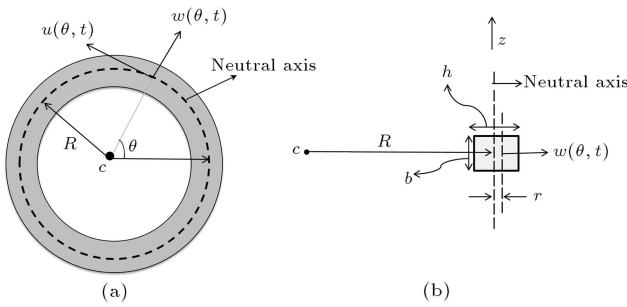


**Figure 1.** Circular micro-ring: (a) Geometry and parameters and (b) ring cross-section.

system is expressed as follows:

$$\begin{cases} u_r = w \\ u_\theta = u + \frac{r}{R}u - \frac{r}{R}\frac{\partial w}{\partial \theta} \\ u_z = 0 \end{cases} \quad (1)$$

where  $u(\theta, t)$  and  $w(\theta, t)$  are displacements in tangential and radial directions, respectively. Furthermore,  $R$  is the ring radius, and  $r$  is the distance of an arbitrary point from the neutral axis of the ring cross-section. Using this displacement field, the non-zero components of the infinitesimal strain tensor, symmetric curvature tensor, and corresponding classical and higher order stresses [34] are calculated as follows:

$$\begin{aligned} \varepsilon_{\theta\theta} &= \frac{1}{R} \frac{\partial u_\theta}{\partial \theta} + \frac{u_r}{R} \\ &= \frac{1}{R} \left[ w + \frac{\partial u}{\partial \theta} + \frac{r}{R} \left( \frac{\partial u}{\partial \theta} - \frac{\partial^2 w}{\partial \theta^2} \right) \right], \end{aligned} \quad (2)$$

$$\chi_{z\theta}^s = \chi_{\theta z}^s = \frac{1}{2R^2} \left( \frac{\partial u}{\partial \theta} - \frac{\partial^2 w}{\partial \theta^2} \right), \quad (3)$$

$$\sigma_{\theta\theta} = \frac{E}{R} \left[ w + \frac{\partial u}{\partial \theta} + \frac{r}{R} \left( \frac{\partial u}{\partial \theta} - \frac{\partial^2 w}{\partial \theta^2} \right) \right], \quad (4)$$

$$m_{z\theta}^s = m_{\theta z}^s = \frac{\mu l^2}{R^2} \left( \frac{\partial u}{\partial \theta} - \frac{\partial^2 w}{\partial \theta^2} \right). \quad (5)$$

In these equations,  $\mu$  is the shear modulus,  $E$  is the modulus of elasticity, and  $l$  is the material length scale parameter. According to the modified couple stress theory [25], the variation of strain energy of the micro ring is obtained as follows:

$$\begin{aligned} \delta U &= \iiint_V (\sigma_{\theta\theta} \delta \varepsilon_{\theta\theta} + 2m_{z\theta} \delta \chi_{z\theta}) dV \\ &= \int_0^{2\pi} \iint_A \left\{ \frac{\sigma_{\theta\theta}}{R} \left( \delta w + \delta \frac{\partial u}{\partial \theta} + \frac{r}{R} \delta \frac{\partial u}{\partial \theta} - \frac{r}{R} \delta \frac{\partial^2 w}{\partial \theta^2} \right) \right. \\ &\quad \left. + 2m_{z\theta} \left( \frac{1}{2R^2} \left( \delta \frac{\partial u}{\partial \theta} - \delta \frac{\partial^2 w}{\partial \theta^2} \right) \right) \right\} R dA d\theta, \end{aligned} \quad (6)$$

in which  $V$  and  $A$  are the volume and ring cross-section,

respectively. The variation of the kinetic energy of the ring is derived as follows:

$$\delta T = -\rho A \int_0^{2\pi} \left[ \frac{\partial^2 w}{\partial t^2} \delta w + \frac{\partial^2 u}{\partial t^2} \delta u \right] R d\theta, \quad (7)$$

where  $\rho$  is the density of micro-ring material. The virtual work done by the external forces acting on the ring is written in the following form.

$$\delta W = \int_0^{2\pi} [f(\theta, t) \delta w + p(\theta, t) \delta u] R d\theta. \quad (8)$$

In the above relation,  $f$  and  $p$  are radial and tangential external forces, respectively. By using the Hamilton's principle, the governing equations of motion of the micro-ring can be derived as follows:

$$\begin{aligned} fR - \frac{EA}{R} \left( w + \frac{\partial u}{\partial \theta} \right) + \left( \frac{EI + \mu Al^2}{R^3} \right) \left( \frac{\partial^3 u}{\partial \theta^3} - \frac{\partial^4 w}{\partial \theta^4} \right) \\ = \rho AR \frac{\partial^2 w}{\partial t^2}, \end{aligned} \quad (9)$$

$$\begin{aligned} pR + \frac{EA}{R} \left( w + \frac{\partial u}{\partial \theta} \right) + \left( \frac{EI + \mu Al^2}{R^3} \right) \left( \frac{\partial^2 u}{\partial \theta^2} - \frac{\partial^3 w}{\partial \theta^3} \right) \\ = \rho AR \frac{\partial^2 u}{\partial t^2}. \end{aligned} \quad (10)$$

Neglecting the length scale parameter reduces the above equation to classic ones reported in the literature [35]. The corresponding boundary conditions are determined as follows:

$$\left( \frac{\partial^2 u}{\partial \theta^2} - \frac{\partial^3 w}{\partial \theta^3} \right) = 0 \quad \text{or} \quad w = \text{const.} @ \theta = 0, 2\pi, \quad (11)$$

$$\frac{EA}{R} \left( w + \frac{\partial u}{\partial \theta} \right) + \left( \frac{EI + \mu Al^2}{R^4} \right) \left( \frac{\partial u}{\partial \theta} - \frac{\partial^2 w}{\partial \theta^2} \right) = 0,$$

or:

$$u = \text{const.} @ \theta = 0, 2\pi, \quad (12)$$

$$\left( \frac{\partial u}{\partial \theta} - \frac{\partial^2 w}{\partial \theta^2} \right) = 0$$

or:

$$\frac{\partial w}{\partial \theta} = \text{const.} @ \theta = 0, 2\pi. \quad (13)$$

### 2.1. Finite-element formulation

Considering the micro-ring neutral axis in-extensionality [35] ( $\varepsilon_{\theta\theta} = 0$ ), the governing equations are reduced to one equation as shown in the following:

$$\begin{aligned} \left( \frac{EI + \mu Al^2}{R^4} \right) \left( \frac{\partial^6 u}{\partial \theta^6} + 2 \frac{\partial^4 u}{\partial \theta^4} + \frac{\partial^2 u}{\partial \theta^2} \right) \\ + \left( p + \frac{\partial f}{\partial \theta} \right) + \rho A \frac{\partial^2}{\partial t^2} \left( \frac{\partial^2 u}{\partial \theta^2} - u \right) = 0. \end{aligned} \quad (14)$$

For the case of electrostatic actuation, the tangential external force ( $p$ ) is considered to be zero, and the radial external force ( $f$ ) is expressed as follows:

$$f = \sum_{j=1}^m \frac{\epsilon_0 A_e V^2}{2 \left(d - \frac{\partial u}{\partial \theta}\right)^2} \left( H \left( \phi_j - \frac{\Delta \phi_j}{2} \right) - H \left( \phi_j + \frac{\Delta \phi_j}{2} \right) \right), \tag{15}$$

where  $m$  is the number of the electrodes,  $\epsilon_0$  is the vacuum permittivity,  $A_e$  is the actuation area of the electrodes facing the ring,  $d$  is the initial gap between the electrodes and the ring, and  $V$  is the applied voltage. Furthermore,  $\phi_j$  and  $\Delta \phi_j$  are the angular position of the  $j$ th electrode center and angular length of the  $j$ th electrode facing the ring perimeter, respectively, and  $H$  is the Heaviside function. The dimensionless parameters are introduced as follows:

$$\hat{u} = \frac{u}{d}, \quad \hat{f} = \frac{f}{EI d / R^4}, \quad \hat{t} = \left( \frac{EI}{\rho A R^4} \right)^{\frac{1}{2}} t, \tag{16}$$

$$\hat{V} = V \sqrt{\frac{\epsilon_0 A_e R^4}{2EI d^3}}.$$

The dimensionless governing equation is obtained as follows:

$$\left( 1 + \frac{\mu A l^2}{EI} \right) \left( \frac{\partial^6 \hat{u}}{\partial \theta^6} + 2 \frac{\partial^4 \hat{u}}{\partial \theta^4} + \frac{\partial^2 \hat{u}}{\partial \theta^2} \right) + \frac{\partial}{\partial \theta} \left( \sum_{j=1}^m \frac{\hat{V}^2}{\left( 1 - \frac{\partial \hat{u}}{\partial \theta} \right)^2} \left( H \left( \phi_j - \frac{\Delta \phi_j}{2} \right) - H \left( \phi_j + \frac{\Delta \phi_j}{2} \right) \right) \right) + \rho A \frac{\partial^2}{\partial t^2} \left( \frac{\partial^2 \hat{u}}{\partial \theta^2} - \hat{u} \right) = 0. \tag{17}$$

In Figure 2, the schematic view of the two-node in-extensional ring element is presented. Parameters  $\theta_1$  and  $\theta_2$  denote the positions of the first and second nodes, while the element length in radian is defined

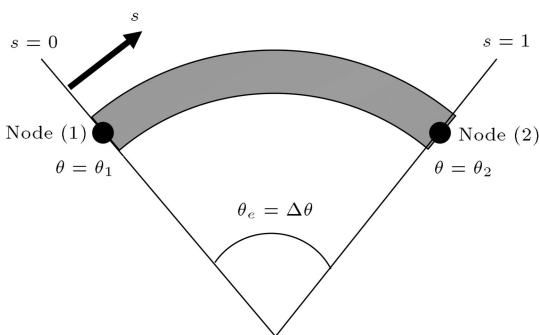


Figure 2. Two-node ring element.

as  $\theta_e = \Delta \theta = \theta_2 - \theta_1$ . The dimensionless coordinate is defined as  $s = (\theta - \theta_1) / \theta_e$ .

According to the governing equation, each node of the element must have 3 degrees of freedom; hence, deflection, slope, and curvature are prescribed at the boundaries. The nodal displacement vector for this new in-extensional size-dependent ring element can be expressed as follows:

$$\delta = \left[ \hat{u}|_1 \quad \frac{\partial \hat{u}}{\partial s} \Big|_1 \quad \frac{\partial^2 \hat{u}}{\partial s^2} \Big|_1 \quad \hat{u}|_2 \quad \frac{\partial \hat{u}}{\partial s} \Big|_2 \quad \frac{\partial^2 \hat{u}}{\partial s^2} \Big|_2 \right]. \tag{18}$$

The nodal displacement is related to the ring displacement using the shape functions as follows:

$$\hat{u}(s, t) = N(s) \delta(t). \tag{19}$$

By utilizing the Hermitian functions, the shape function vector ( $N$ ) is defined as follows: :

$$N_1 = 1 - 10s^3 + 15s^4 - 6s^5, \tag{20}$$

$$N_2 = \theta_e (s - 6s^3 + 8s^4 - 3s^5),$$

$$N_3 = \theta_e^2 \left( \frac{1}{2} s^2 - \frac{3}{2} s^3 + \frac{3}{2} s^4 - \frac{1}{2} s^5 \right),$$

$$N_4 = 10s^3 - 15s^4 + 6s^5,$$

$$N_5 = \theta_e (-4s^3 + 7s^4 - 3s^5),$$

$$N_6 = \theta_e^2 \left( \frac{1}{2} s^3 - s^4 + \frac{1}{2} s^5 \right).$$

Using the Galerkin method [36], the proposed nodal displacement, the corresponding shape functions, and some mathematical manipulations, the governing equation in the matrix form for one element is obtained as follows:

$$[M] [\ddot{\delta}] + [K] [\delta] = [F_e], \tag{21}$$

where  $[M] = [M_1] + [M_2]$  and  $[K] = [K_1] + [K_2] + [K_3]$  are mass and stiffness matrices, respectively, which are obtained by Eqs. (22) to (26) as shown in Box I. The external force acting on the ring element can be expressed as follows:

$$F_e = \int_0^1 \left( \left[ \frac{dN}{ds} \right]^T \left( \frac{\hat{V}^2}{\left( 1 - \frac{1}{\theta_e} \frac{\partial \hat{u}}{\partial s} \right)^2} \right) \right) ds. \tag{27}$$

It should be noted that the electrostatic DC voltage is considered only for the elements facing the electrodes.

$$K_1 = \frac{1}{2520(\theta_e)} \begin{bmatrix} 3600 & 540\theta_e & 30\theta_e^2 & -3600 & 540\theta_e & 30\theta_e^2 \\ 540\theta_e & 576\theta_e^2 & 42\theta_e^3 & -540\theta_e & -36\theta_e^2 & 12\theta_e^3 \\ 30\theta_e^2 & 42\theta_e^3 & 4\theta_e^4 & -30\theta_e^2 & -12\theta_e^3 & 2\theta_e^4 \\ -3600 & -540\theta_e & -30\theta_e^2 & 3600 & -540\theta_e & 30\theta_e^2 \\ 540\theta_e & -36\theta_e^2 & -12\theta_e^3 & -540\theta_e & 576\theta_e^2 & -42\theta_e^3 \\ -30\theta_e^2 & 12\theta_e^3 & 2\theta_e^4 & 30\theta_e^2 & -42\theta_e^3 & 4\theta_e^4 \end{bmatrix} \left(1 + \frac{\mu A l^2}{EI}\right), \quad (22)$$

$$K_2 = \frac{-2}{70(\theta_e^3)} \begin{bmatrix} 1200 & 600\theta_e & 30\theta_e^2 & -1200 & 600\theta_e & -30\theta_e^2 \\ 600\theta_e & 384\theta_e^2 & 22\theta_e^3 & -600\theta_e & 216\theta_e^2 & -8\theta_e^3 \\ 30\theta_e^2 & 22\theta_e^3 & 6\theta_e^4 & -30\theta_e^2 & 8\theta_e^3 & \theta_e^4 \\ -1200 & -600\theta_e & -30\theta_e^2 & 1200 & -600\theta_e & 30\theta_e^2 \\ 600\theta_e & 216\theta_e^2 & 8\theta_e^3 & -600\theta_e & 384\theta_e^2 & -22\theta_e^3 \\ -30\theta_e^2 & -8\theta_e^3 & \theta_e^4 & 30\theta_e^2 & -22\theta_e^3 & 6\theta_e^4 \end{bmatrix} \left(1 + \frac{\mu A l^2}{EI}\right), \quad (23)$$

$$K_3 = \frac{1}{(\theta_e^5)} \begin{bmatrix} 720 & 360\theta_e & 60\theta_e^2 & -720 & 360\theta_e & -60\theta_e^2 \\ 360\theta_e & 192\theta_e^2 & 36\theta_e^3 & -360\theta_e & 168\theta_e^2 & -24\theta_e^3 \\ 60\theta_e^2 & 36\theta_e^3 & 9\theta_e^4 & -60\theta_e^2 & 24\theta_e^3 & -3\theta_e^4 \\ -720 & -360\theta_e & -60\theta_e^2 & 720 & -360\theta_e & 60\theta_e^2 \\ 360\theta_e & 168\theta_e^2 & 24\theta_e^3 & -360\theta_e & 192\theta_e^2 & -36\theta_e^3 \\ -60\theta_e^2 & -24\theta_e^3 & -3\theta_e^4 & 60\theta_e^2 & -36\theta_e^3 & 9\theta_e^4 \end{bmatrix} \left(1 + \frac{\mu A l^2}{EI}\right), \quad (24)$$

$$M_1 = \frac{\theta_e}{55440} \begin{bmatrix} 21720 & 3732\theta_e & 281\theta_e^2 & 6000 & -1812\theta_e & 181\theta_e^2 \\ 3732\theta_e & 832\theta_e^2 & 69\theta_e^3 & 1812\theta_e & -532\theta_e^2 & 52\theta_e^3 \\ 281\theta_e^2 & 69\theta_e^3 & 6\theta_e^4 & 181\theta_e^2 & -52\theta_e^3 & 5\theta_e^4 \\ 6000 & 1812\theta_e & 181\theta_e^2 & 21720 & -3732\theta_e & 281\theta_e^2 \\ -1812\theta_e & -532\theta_e^2 & -52\theta_e^3 & -3732\theta_e & 832\theta_e^2 & -69\theta_e^3 \\ 181\theta_e^2 & 52\theta_e^3 & 5\theta_e^4 & 281\theta_e^2 & -69\theta_e^3 & 6\theta_e^4 \end{bmatrix}, \quad (25)$$

$$M_2 = \frac{1}{2520(\theta_e)} \begin{bmatrix} 3600 & 540\theta_e & 30\theta_e^2 & -3600 & 540\theta_e & 30\theta_e^2 \\ 540\theta_e & 576\theta_e^2 & 42\theta_e^3 & -540\theta_e & -36\theta_e^2 & 12\theta_e^3 \\ 30\theta_e^2 & 42\theta_e^3 & 4\theta_e^4 & -30\theta_e^2 & -12\theta_e^3 & 2\theta_e^4 \\ -3600 & -540\theta_e & -30\theta_e^2 & 3600 & -540\theta_e & 30\theta_e^2 \\ 540\theta_e & -36\theta_e^2 & -12\theta_e^3 & -540\theta_e & 576\theta_e^2 & -42\theta_e^3 \\ -30\theta_e^2 & 12\theta_e^3 & 2\theta_e^4 & 30\theta_e^2 & -42\theta_e^3 & 4\theta_e^4 \end{bmatrix}. \quad (26)$$

Box I

**2.2. Linear natural frequency**

The natural frequency of the gyroscope under applied DC voltage is investigated in this section. Therefore, it is considered that the micro-ring has small dynamic deformation (vibration) around its static deflection (calculated in the previous section by neglecting time dependent terms). The total deflection of the micro-ring can be presented as follows:

$$\hat{u}(\theta, t) = \hat{u}_s(\theta) + \hat{u}_d(\theta, t), \quad (28)$$

where  $\hat{u}_s$  and  $\hat{u}_d$  are static and dynamic deflections of the structure. Substituting the above-mentioned deformation and utilizing the Taylor expansion for the electrostatic load yields the following:

$$\begin{aligned} & \left(1 + \frac{\mu A l^2}{EI}\right) \left( \frac{\partial^6 (\hat{u}_s + \hat{u}_d)}{\partial \theta^6} + 2 \frac{\partial^4 (\hat{u}_s + \hat{u}_d)}{\partial \theta^4} + \frac{\partial^2 (\hat{u}_s + \hat{u}_d)}{\partial \theta^2} \right) \\ & + \frac{\partial}{\partial \theta} \left( \sum_{j=1}^m \left( \sum_{m=0}^{\infty} \frac{\hat{V}^2(m+1)}{(1 - \frac{\partial \hat{u}_s}{\partial \theta})^{m+2}} \left( \frac{\partial \hat{u}_d}{\partial \theta} \right)^m \right) \right) \\ & \left( H \left( \phi_j - \frac{\Delta \phi_j}{2} \right) - H \left( \phi_j + \frac{\Delta \phi_j}{2} \right) \right) \\ & + \rho A \frac{\partial^2}{\partial t^2} \left( \frac{\partial^2 (\hat{u}_d)}{\partial \theta^2} - (\hat{u}_d) \right) = 0. \end{aligned} \quad (29)$$

For small vibration of micro-ring around the static deflection, the linear natural frequency can be considered

as the resonant frequency of the system with negligible error [37]. Using the proposed finite-element formulation and omitting the static deformation results, the linear natural frequency of the system under applied DC voltage can be studied. By assuming the dynamic deformation similar to Eq. (19), the matrix form of the equation for one element is obtained as follows:

$$[M] \{\delta\} + ([K] + [K_{DC}]) \{\delta\} = 0. \tag{30}$$

The matrices  $[M]$  and  $[K]$  where derived in the previous section, and  $[K_{DC}]$  of the ring element can be obtained as follows:

$$K_{DC} = - \int_0^1 \left( \left[ \frac{dN}{ds} \right]^T \left( \frac{2\hat{V}^2}{\left(1 - \frac{1}{\theta_c} \frac{\partial \hat{u}_s}{\partial s}\right)^3} \right) \left[ \frac{dN}{ds} \right] \right) ds. \tag{31}$$

By assembling the mass and stiffness matrices along with the force vectors of all elements and satisfying the boundary conditions, the complete model of the structure (i.e., the main micro ring and the eight half circular stiffeners) can be obtained; based on the actuation electrodes position, the static DC voltage can be employed for the FE model.

### 3. Results and discussion

The vibrating ring gyroscope is assumed to be made of polysilicon. The density, Young modulus, and shear modulus of elasticity for polysilicon are considered as  $\rho = 2332 \text{ kg/m}^3$ ,  $E = 150 \text{ GPa}$ , and  $\mu = 60.98 \text{ GPa}$ , respectively [38,39]. Figure 3 shows excellent match between the analytically [35,40] and numerically obtained (present work) first natural frequencies of single micro ring (i.e., the ring without stiffness). Based on this agreement, for more complicated systems (such as

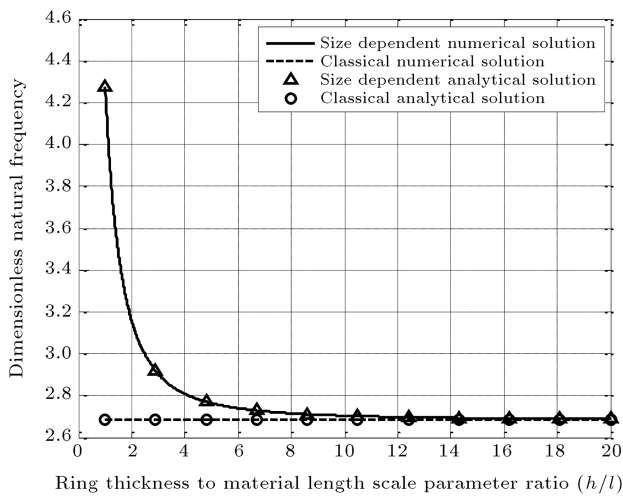


**Figure 3.** First numerical and analytical natural frequency of the micro-ring.

the ring with stiffeners) in which analytical method is not applicable, using finite-element analysis and the proposed element gives favorable evaluation of the behavior of the system. In addition, this figure indicates that the proposed ring element captures the size-dependent behavior of the micro rings, revealing that the element is suitable for modeling of the micro scale systems.

In Figure 4, the first natural frequency of complete non-classic structure (micro ring and stiffeners) is presented for different ring thickness to material length scale parameter ratios. This figure obviously shows the size-dependent behavior of vibrating ring gyroscope when the ring thickness and material length scale parameter are in the same order. As this ratio increases, the non-classic results converge to classic ones. By using the finite-element model presented in this paper, the mode shapes of the ring gyroscope are obtained. In the previous researches on the vibrating ring gyroscopes [12,41], the mode shape of the system is considered similar to that of single ring [35] (i.e.,  $\sin(n\theta)$ ), while Figure 5 shows that the mode shape of the gyroscope is slightly different from the assumed mode shapes presented in the literature. This finding reveals that in order to obtain highly accurate behavior and response of the vibrating ring gyroscope, the presented mode shape should be utilized.

The actuation force applied to the vibrating ring gyroscopes is a combination of DC and AC electrostatic forces. Since the DC voltage can cause a frequency change in micro electromechanical systems and also the static pull-in voltage is an important characteristic parameter of MEMS devices in the following figures, the effect of applying static DC voltage on the behavior of the ring gyroscope for two different electrodes orientation is analyzed. The first two modes of the vibrating micro ring gyroscope have equal natural frequencies

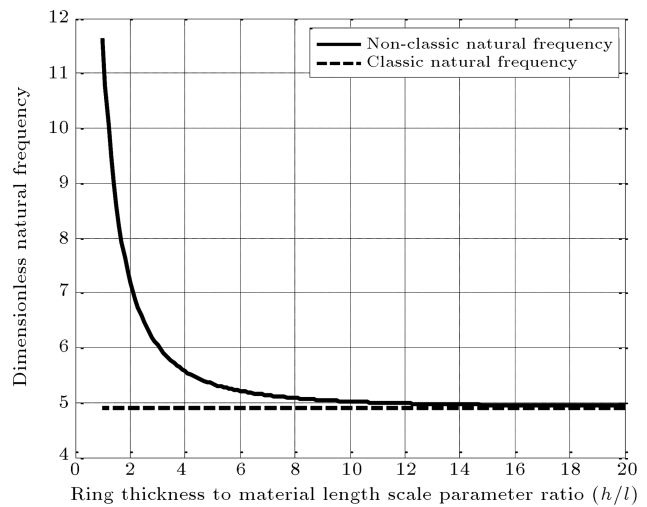


**Figure 4.** Comparison of the first classical and non-classical natural frequencies of the ring with stiffeners.

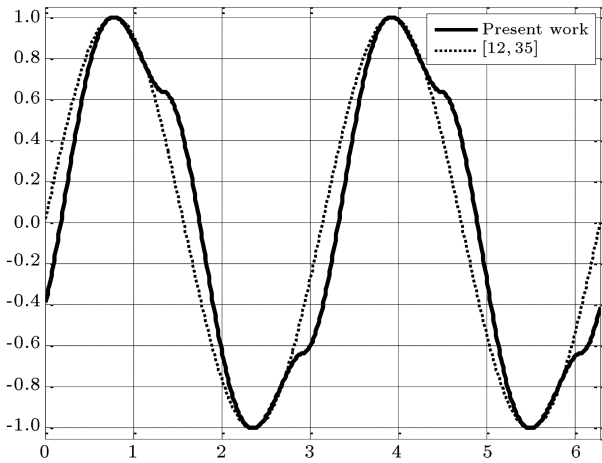


Figure 5. First mode shape of the ring gyroscope.

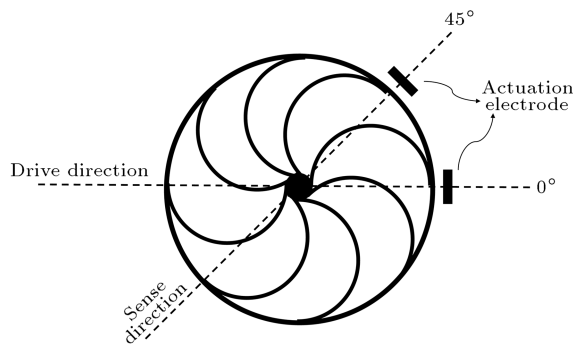


Figure 6. Main ring on eight stiffeners and orientation of electrodes in the sense and drive directions.

with different mode shapes. These modes are in  $45^\circ$  shift on the ring perimeter where the drive and sense directions of the gyroscope are placed in the direction of these modes. Actuation electrodes are considered for applying DC voltage in two different orientations. In the first orientation, as it is shown in Figure 6, the actuation electrode for DC voltage is located in the first mode direction ( $0^\circ$ ). In the second orientation, the actuation electrodes are positioned in  $0^\circ$  and  $45^\circ$  where one of them is in the first mode and the other one in the second mode direction. The angular length of each electrode is assumed to be  $2^\circ$ .

The linear natural frequency of the ring gyroscope under application of electrostatic DC voltage for the first orientation of electrodes is presented in Figure 7. Different values for the ring thickness to material length scale parameter ratio ( $h/l=3, 5$  and  $h/l > 100$ ) are considered, and size-dependent behavior of the gyroscope is observed clearly. Moreover, applying DC voltage caused a frequency split between the natural frequency of the system in the 1st (drive) and 2nd (sense) modes, which are important to be equal for vibrating ring gyroscopes. In Figure 8, the natural frequency of the complete ring for the second orientation of the actuated electrodes for different ratios of ring

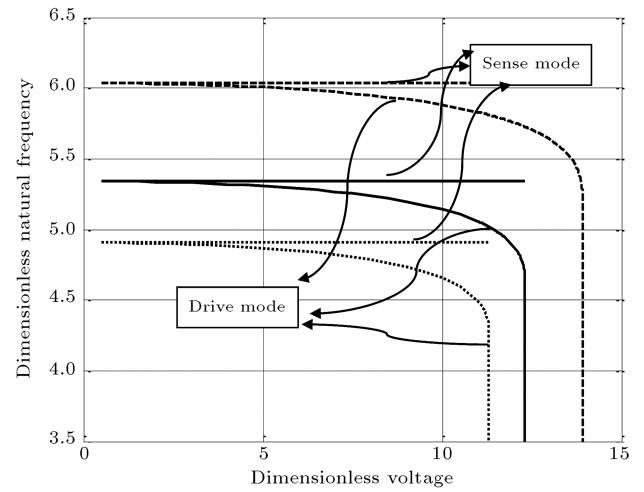


Figure 7. Natural frequency for actuated electrode in  $0^\circ$  (---  $h/l = 3$ , -  $h/l = 5$ , ...  $h/l \gg 100$ ).

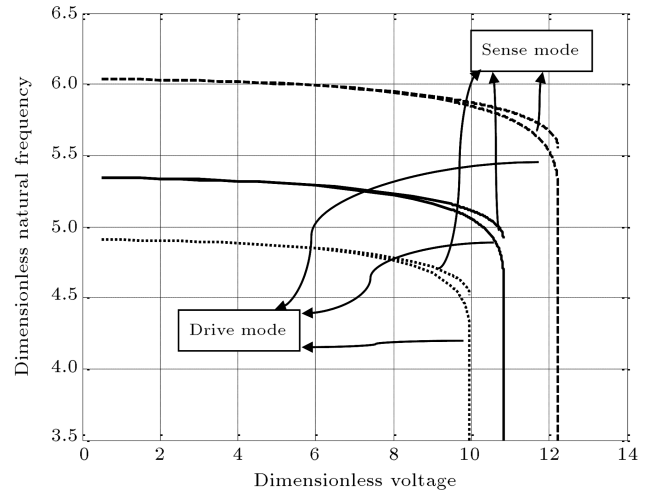
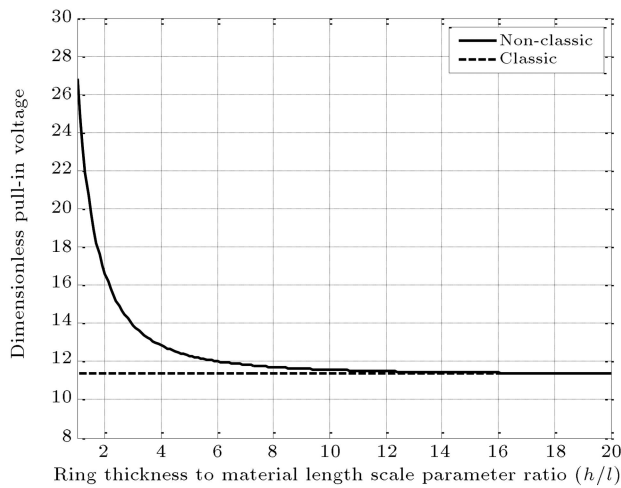


Figure 8. Natural frequency for actuated electrodes in  $0^\circ$  and  $45^\circ$  (---  $h/l = 3$ , -  $h/l = 5$ , ...  $h/l \gg 100$ ).

thickness to material length scale parameter ( $h/l=3, 5$  and  $h/l > 100$ ) is illustrated. Since the DC voltage is applied to the ring in both sense and drive directions, the frequency split of the ring happens just near pull-in voltage.

Pull-in instability and pull-in voltage of the complete ring gyroscope for the first and second orientations of electrodes with respect to the ratio of ring thickness to material length scale parameter are plotted in Figures 9 and 10. A comparison of these figures reveals that, for the second orientation of the electrodes, the pull-in voltage is lower than the first orientation, meaning that lower DC voltage must be applied to the system for the second orientation in order to expect linear behavior for the system. In addition to that, the size-dependent behavior of the ring gyroscope is found from these figures, which indicate that when the ring thickness is in order of material length scale parameter,



**Figure 9.** Pull-in voltage versus ring thickness to material length scale ratio for actuated electrode in  $0^\circ$ .

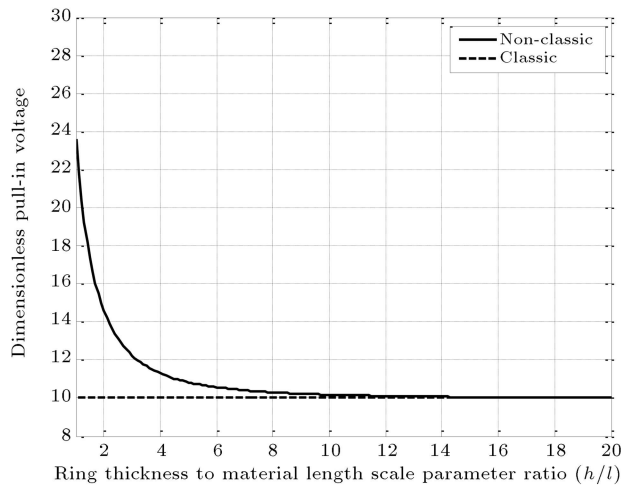


**Figure 10.** Pull-in voltage versus ring thickness to material length scale ratio for actuated electrodes in  $0^\circ$  and  $45^\circ$ .

the classic and non-classic responses have a meaningful difference.

The maximum deflection of the size-dependent ring gyroscope under application of DC voltage for two different orientations of electrodes is presented in Figures 11 and 12. Results reveal that as the ring thickness to material length scale parameter ratio increases, the size dependency effect decreases, and classical and non-classical findings converge together. The comparison of these figures can determine the difference between pull-in voltage and maximum deflection of complete ring with respect to the two methods of applying DC voltage.

#### 4. Conclusion

The governing equations of the size-dependent micro ring based on the modified couple stress theory and

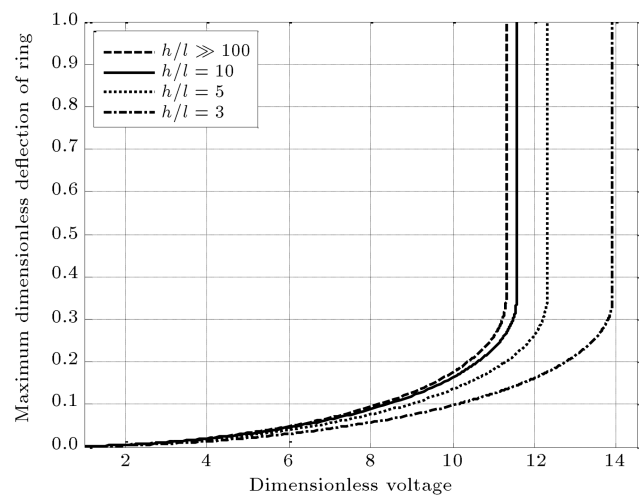


**Figure 11.** Maximum deflection of ring versus pull-in voltage for actuated electrodes in  $0^\circ$ .

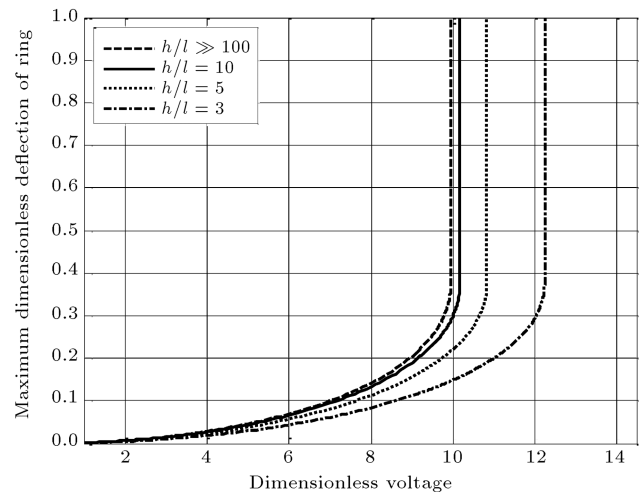


**Figure 12.** Maximum deflection of ring versus pull-in voltage for actuated electrodes in  $0^\circ$  and  $45^\circ$ .

Hamilton's principle were derived in this work. By considering the in-extensionality of the micro ring and using the derived governing equations, the finite-element model of the vibrating ring gyroscope (circular micro ring along with eight half circular stiffeners) (ring gyroscope) was developed. The natural frequency analysis of the micro-ring gyroscope was performed, and precise mode shape of the system was achieved, which is slightly different from the mode shapes proposed in the literature. Response of the gyroscope under application of electrostatic DC voltage was investigated, and static deflection, maximum deflection of ring, and pull-in voltage were obtained. Two different orientations for the actuation electrodes of the micro ring gyroscope (namely  $0^\circ$  and  $0^\circ$  &  $45^\circ$ ) were considered, and the effect of these orientations on the device frequencies in sense and drive directions along with the static pull-in instability was investigated. Findings confirmed the

size-dependent behavior of the micro gyroscope and showed the gap between the classic and non-classic natural frequencies and static pull-in voltage of the gyroscope when the ring thickness was in order of material length scale parameter. The numerically obtained first natural frequency of the finite-element model of single micro-ring was compared to analytical natural frequency of the model, and excellent agreement was observed.

## References

- Bogue, R. "Recent developments in MEMS sensors: A review of applications, markets, and technologies", *Sensor Rev.*, **33**(4), pp. 300-304 (2013).
- Karimzade, A., Ahmadian, M.T. and Asemani, H. "Nonlinear analysis of pull-in phenomenon and maximum deflection of MEMS with movable base under capillary and Van Der Waals forces", In *Int. Mech. Eng. Cong. and Expo. (IMECE)*: American Society of Mechanical Engineers (2012).
- Karimzade, A., Moeenfard, H., and Ahmadian, M.T. "Nonlinear analysis of pull-in voltage for a fully clamped microplate with movable base", In *Int. Mech. Eng. Cong. And Expo. (IMECE)*: American Society of Mechanical Engineers (2012).
- Zuo, W., Li, P., Fang, Y., et al. "Thermoelastic damping in asymmetric three-layered microbeam resonators", *J. Appl. Mech.*, **83**(6), p. 061002 (2016).
- Pasharavesh, A. and Ahmadian, M.T. "Characterization of a nonlinear MEMS-based piezoelectric resonator for wideband micro power generation", *Appl. Math. Model.*, **41**, pp. 121-142 (2017).
- Pasharavesh, A., Ahmadian, M.T., and Zohoor, H. "Electromechanical modeling and analytical investigation of nonlinearities in energy harvesting piezoelectric beams", *Int. J. Mech. Mater. Des.*, **13**(4), pp. 1-16 (2017).
- Yazdi, N., Ayazi, F., and Najafi, K. "Micromachined inertial sensors", *Proceedings of the IEEE.*, **86**(8), pp. 1640-1659 (1998).
- Dao, D.V., Nakamura, K., Bui, T.T., et al. "Micro/nano-mechanical sensors and actuators based on SOI-MEMS technology", *Adv. Nat. Sci.: Nanosci. Nanotech.*, **1**(1), pp. 013001 (2010).
- Trusov, A.A., Prikhodko, I.P., Zotov, S.A., et al. "Low-dissipation silicon tuning fork gyroscopes for rate and whole angle measurements", *IEEE Sensors J.*, **11**(11), pp. 2763-2770 (2011).
- Ghommam, M., Nayfeh, A.H., Choura, S., et al. "Modeling and performance study of a beam microgyroscope", *J. Sound Vib.*, **329**(23), pp. 4970-4979 (2010).
- Ayazi, F. and Najafi, K. "A HARPSS polysilicon vibrating ring gyroscope", *J. Microelectromech. Sys.*, **10**(2), pp. 169-179 (2001).
- Tao, Y., Wu, X., Xiao, D., et al. "Design, analysis and experiment of a novel ring vibratory gyroscope", *Sensor. Actuat. A-Phys.*, **168**(2), pp. 286-299 (2011).
- Zaman, M.F., Sharma, A., Amini, B.V., et al. "The resonating star gyroscope", In *18th IEEE Int. Conf. Micro Electro Mech. Sys.*, IEEE (2005).
- Putty, M.W., *Micromachined Vibrating Ring Gyroscope*, University of Michigan (1995).
- Weng, J.-H., Chieng, W.-H., and Lai, J.-M. "Structural design and analysis of micromachined ring-type vibrating sensor of both yaw rate and linear acceleration", *Sensor. Actuat. A-Phys.*, **117**(2), pp. 230-240 (2005).
- Wu, X. and Parker, R.G. "Vibration of rings on a general elastic foundation", *J. Sound Vib.*, **295**(1), pp. 194-213 (2006).
- Cooley, C.G. and Parker, R.G. "Vibration of high-speed rotating rings coupled to space-fixed stiffnesses", *J. Sound Vib.*, **333**(12), pp. 2631-2648 (2014).
- Lacarbonara, W., Arena, A., and Antman, S.S. "Flexural vibrations of nonlinearly elastic circular rings", *Meccanica.*, **50**(3), pp. 1-17 (2014).
- Karimzadeh, A., Ahmadian, M.T., Firoozbakhsh, K., et al. "Vibrational analysis of size-dependent rotating micro-rings", *Int. J. Struct. Stab. Dyn.*, **17**(9), p. 1771012 (2017).
- Huang, D., Tang, L., and Cao, R. "Free vibration analysis of planar rotating rings by wave propagation", *J. Sound Vib.*, **332**(20), pp. 4979-4997 (2013).
- Bisegna, P. and Caruso, G. "Frequency split and vibration localization in imperfect rings", *J. Sound Vib.*, **306**(3), pp. 691-711 (2007).
- McFarland, A.W. and Colton, J.S. "Role of material microstructure in plate stiffness with relevance to microcantilever sensors", *J. Micromech. Microeng.*, **15**(5), pp. 1060 (2005).
- Liu, D., He, Y., Dunstan, D.J., et al. "Toward a further understanding of size effects in the torsion of thin metal wires: an experimental and theoretical assessment", *Int. J. Plasticity*, **41**, pp. 30-52 (2013).
- Stölken, J.S. and Evans, A.G. "A microbend test method for measuring the plasticity length scale", *Acta Mater.*, **46**(14), pp. 5109-5115 (1998).
- Yang, F., Chong, A.C.M., Lam, D.C.C., et al. "Couple stress based strain gradient theory for elasticity", *Int. J. Solid. Struct.*, **39**(10), pp. 2731-2743 (2002).
- Kim, J. and Reddy, J.N. "A general third-order theory of functionally graded plates with modified couple stress effect and the von Kármán nonlinearity: theory and finite element analysis", *Acta Mech.*, **226**(9), p. 2973 (2015).
- Rahaeifard, M., Kahrobaian, M.H., Asghari, M., et al. "Static pull-in analysis of microcantilevers based on the modified couple stress theory", *Sensor. Actuat. A-Phys.*, **171**(2), pp. 370-374 (2011).

28. Mojahedi, M. and Rahaeifard, M. “Static deflection and pull-in instability of the electrostatically actuated bilayer microcantilever beams”, *Int. J. Appl. Mech.*, **7**(06), p. 1550090 (2015).
29. Osterberg, P.M. and Senturia, S.D. “M-TEST: a test chip for MEMS material property measurement using electrostatically actuated test structures”, *J. Microelectromech. Sys.*, **6**(2), pp. 107-118 (1997).
30. Abbasnejad, B., Rezazadeh, G., and Shabani, R. “Stability analysis of a capacitive fgm micro-beam using modified couple stress theory”, *Acta Mech. Solida Sinica*, **26**(4), pp. 427-440 (2013).
31. Wang, K.F., Kitamura, T., and Wang, B. “Non-linear pull-in instability and free vibration of micro/nanoscale plates with surface energy - A modified couple stress theory model”, *Int. J. Mech. Sci.*, **99**, pp. 288-296 (2015).
32. Zhang, J. and Fu, Y. “Pull-in analysis of electrically actuated viscoelastic microbeams based on a modified couple stress theory”, *Meccanica*, **47**(7), pp. 1649-1658 (2012).
33. Rahaeifard, M. and Mojahedi, M. “Size-dependent dynamic behavior of electrostatically actuated microaccelerometers under mechanical shock”, *Int. J. Struct. Stab. Dyn.*, **16**, p. 1750042 (2016).
34. Ashoori, A. and Mahmoodi, M.J. “The modified version of strain gradient and couple stress theories in general curvilinear coordinates”, *Eur. J. Mech. A-Solids*, **49**, pp. 441-454 (2015).
35. Rao, S.S., *Vibration of Continuous Systems*, New York: John Wiley & Sons (2007).
36. Huebner, K.H., Dewhurst, D.L., Smith, D.E., et al., *The Finite Element Method for Engineers*, John Wiley & Sons (2008).
37. Abdel-Rahman, E.M., Younis, M.I., and Nayfeh, A.H. “Characterization of the mechanical behavior of an electrically actuated microbeam”, *J. Micromech. Microeng.*, **12**(6), pp. 759 (2002).
38. Tilmans, H.A.C. and Legtenberg, R. “Electrostatically driven vacuum-encapsulated polysilicon resonators: Part II. Theory and performance”, *Sensor. Actuat. A-Phys.*, **45**(1), pp. 67-84 (1994).
39. Fischer, D.S., *Development of In-situ Toughened Silicon-rich Alloys: A New Class of Castable Engineering Ceramics*, In Department of Materials Science and Engineering, Massachusetts Institute of Technology (2010).
40. Karimzadeh, A., Ahmadian, M.T., and Rahaeifard, M. “Effect of size dependency on in-plane vibration of circular micro-rings”, *Sci. Iran. Trans. B*, **24**(4), pp. 1996-2008 (2017).
41. Esmaeili, M., Durali, M., and Jalili, N. “Ring micro-gyroscope modeling and performance evaluation”, *J. Vib. Control*, **12**(5), pp. 537-553 (2006).

## Biographies

**Ali Karimzadeh** was born in 1988. He received his BS degree in Mechanical Engineering from the University of Shiraz, Iran in 2010 and the MS degree in the same field of study from the Sharif University of Technology in 2012. He received his PhD degree from the School of Mechanical Engineering from Sharif University of Technology in 2018. His research interests include micro electromechanical systems, dynamic and vibration, and advanced finite-element method.

**Mohammad Taghi Ahmadian** received a PhD degree from the Department of Mechanical Engineering at the University of Kansas, USA in 1986. From 1984 to 1985, he was an Assistant Professor at the University of Missouri, and from 1985 to 1988, he was an Assistant Professor at the Department of Mechanical Engineering at the University of Kansas at Lawrence. He started working as an Assistant Professor at Sharif University of Technology from 1989; at present, he is a Professor in the School of Mechanical Engineering at Sharif University of Technology, Tehran. His research interests include cellular biomechanics, soft tissue modeling, strength of material, and advanced finite-element method.